Acta Cryst. (1983). B**39**, 145–153

X-ray Diffraction Study of Short-Range Order in a Disordered Au_3Cu Alloy

BY M. BESSIÈRE, S. LEFEBVRE AND Y. CALVAYRAC

CECM, 15, rue G. Urbain, 94400 Vitry-sur-Seine, France

(*Received* 5 *March* 1982; *accepted* 21 *September* 1982)

Abstract

The X-ray diffuse scattering from an Au_3Cu single crystal rapidly cooled from 485 K is quantitatively measured both at room temperature and at 80 K. Different methods for correcting from temperature diffuse scattering are used: extrapolation to 0 K, calculation of thermal diffuse scattering [Walker & Chipman (1970). *Acta Cryst.* A**26**, 447–455], data analysis with the Borie–Sparks method [Borie & Sparks (1971). *Acta Cryst.* A**27**, 198–201] and with the improvement proposed by Hayakawa, Bardhan & Cohen [*J. Appl. Cryst.* (1975). **8**, 87–95]. As in earlier electron diffraction studies [Watanabe & Fischer (1965). *J. Phys. Soc. Jpn*, **20**, 2170–2179], a fourfold splitting of the diffuse intensity is observed at 100, 110 and equivalent positions in reciprocal space. A recalculated short-range-order intensity map shows that long-range two-site correlation functions are essential in order to fit the experimental data.

Introduction

The copper–gold system which exemplifies order–disorder transitions has been the subject of many investigations.

The phase diagram presents three ordered phases around stoichiometric compositions Cu_3Au, CuAu, Au_3Cu at 661, 693 and 473 K respectively. In addition to the usual ordered structures, one-dimensional periodic antiphase structures (PAP) are observed in almost all the upper part of the ordered regions in the phase diagram (Fig. 1).

For the particular case of the gold-rich region, the low value of the transition temperature (Hirabayashi, 1959) has led in the past to some misleading interpretations (Sato & Toth, 1966; Watanabe & Fischer, 1965). Actually electron diffraction studies have demonstrated that, as for $Cu_{0.7}Au_{0.3}$, the ordered phases do exhibit both PAP and $L1_2$ structures (Gratias, Condat & Fayard, 1972).

An X-ray study of Au_3Cu in both disordered and ordered states has been done by Batterman (1957). Short-range-order (SRO) parameters have been determined from samples held at 523 and 593 K and also from samples quenched from 558 K. The SRO diffuse intensity distribution of this X-ray study showed an egg-shaped intensity distribution located around the superlattice position and with the major axis along the line between the two nearest fundamental reflections.

A more precise picture of the SRO diffuse intensity has been obtained by electron microscopy: Watanabe & Fischer (1965) have observed a splitting into four diffuse spots around the ⟨110⟩ superlattice position. They explained the discrepancies between X-ray and electron diffraction observations by a lack of resolution in the X-ray experiment.

However, advances both in the resolution of the X-ray spectrometers and in data analysis should allow the splitting by X-ray diffraction to be seen. This fourfold splitting of the SRO diffuse intensity distribution has been seen in other disordered alloys by electron diffraction (Cu_3Au: Hashimoto & Ogawa, 1970; CuAu: Sato, Watanabe & Ogawa, 1962; Cu_3Pd: Ohshima & Watanabe, 1973) and by X-ray diffusion (Cu_3Au: Moss, 1966*a*,*b*; AuPd: Linn, Spruiell & Williams, 1970; Cu_3Pd: Ohshima, Watanabe & Harada, 1976; CuAl: Epperson, Fürnrohr & Ortiz, 1978).

In the present paper we report the results of X-ray measurements obtained from a disordered Au_3Cu alloy cooled from 485 K. It is shown that the fourfold splitting of the SRO diffuse scattering at the superstructure reciprocal-lattice points can be observed due

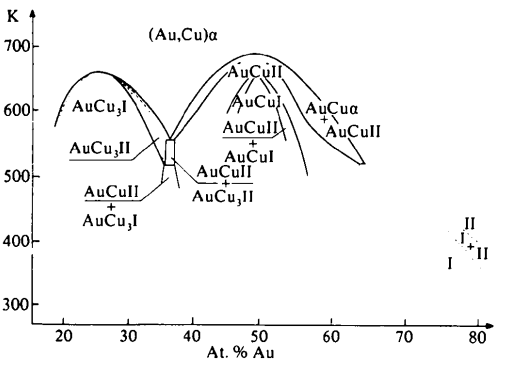

Fig. 1. Phase diagram of Cu–Au alloy.

0567-7408/83/020145-09$01.50

to the good resolution of this X-ray experiment. The SRO and the size-effect parameters, as well as the pair-interaction potentials have been determined.

Experimental procedure

The Au_3Cu alloy is prepared by melting 99·999% Au and ASARCO 99·999% Cu under secondary vacuum. The single crystal is grown in a graphite crucible under vacuum by a horizontal Bridgman technique. It is then homogenized by annealing for 2 h at 1258 K and slowly cooled to room temperature. A slab (14 mm in diameter and 2 mm in thickness) is cut from the ingot by spark machining. The surface is close to a (115) plane. The sample is finally annealed for 1 h at 483 K under secondary vacuum and air cooled. The lattice parameter is $a = 4{\cdot}023$ Å (Pearson, 1958).

The diffractometer used for the diffuse scattering measurement has been described elsewhere (Bessière, Lefebvre, Calvayrac, Bley & Fayard, 1982). The cobalt $K\alpha$ radiation is focused at the receiving slits by a doubly bent pyrolitic graphite monochromator. The second- and higher-order harmonic components are eliminated using a Si(Li) solid-state detector. The beam divergencies are adjusted to allow measurements of diffuse intensity at points in reciprocal space separated by $\Delta h = 0{\cdot}1$ reciprocal-lattice unit (r.l.u.). The measurements are performed up to 0·25 r.l.u. around the Bragg peaks. The intensity of the direct beam is measured by the integrated intensities of diffraction lines of a standard Ni_3Fe briquet. The crystal is mounted on a specially designed cryostat allowing measurements at 80 K and room temperature.

The Compton scattering effect is eliminated from the intensity data after conversion to absolute electron units. It is calculated from Cromer & Mann (1967).

Data analysis

The total diffuse intensity I_D is due to the modulations of the Laue intensity by the short-range order (I_{SRO}) plus the contributions resulting from static (first and second order) and thermal displacements of atoms. According to Borie & Sparks (1971) the intensity may be expanded as:

$$\frac{I_D}{NC_AC_B(f_A - f_B)^2} = I_{\mathrm{SRO}} + I_1 + I_2, \qquad (1)$$

where N is the total number of irradiated atoms, C_A and C_B are the concentrations of A and B chemical species, the atomic scattering factors of which are respectively f_A and f_B.

I_1 is the first-order intensity due to static displacements of the atoms from the sites of the undistorted lattice (size-effect modulation term) and I_2 the second-order intensity (including dynamic displacements). The atomic displacement $\mathbf{\Delta}$ and the diffraction vector $\mathbf{k}$ must be sufficiently small so that terms of higher order may be neglected.

The different components showing different symmetries, they may be differentiated following the method developed by Gragg & Cohen (1971). The volume of measurement was sampled in reciprocal space at 1500 points at intervals of 0·1 r.l.u.

Each term in (1) is written as a series:

$$I_{\mathrm{SRO}} = \sum_l \sum_m \sum_n \alpha_{lmn} \cos \pi l h_1 \cos \pi m h_2 \cos \pi n h_3 \quad (2)$$

$$\begin{aligned} I_1 = \sum_l \sum_m \sum_n (&h_1 \gamma^x_{lmn} \sin \pi l h_1 \cos \pi m h_2 \cos \pi n h_3 \\ &+ h_2 \gamma^y_{lmn} \cos \pi l h_1 \sin \pi m h_2 \cos \pi n h_3 \\ &+ h_3 \gamma^z_{lmn} \cos \pi l h_1 \cos \pi m h_2 \sin \pi n h_3) \end{aligned} \quad (3)$$

$$\begin{aligned} I_2 = \sum_l \sum_m \sum_n \big|&(h_1^2 \delta^x_{lmn} + h_2^2 \delta^y_{lmn} + h_3^2 \delta^z_{lmn} \\ &\times \cos \pi l h_1 \cos \pi m h_2 \cos \pi n h_3 \\ &+ h_1 h_2 \varepsilon^{xy}_{lmn} \sin \pi l h_1 \sin \pi m h_2 \cos \pi n h_3 \\ &+ h_2 h_3 \varepsilon^{yz}_{lmn} \cos \pi l h_1 \sin \pi m h_2 \sin \pi n h_3 \\ &+ h_3 h_1 \varepsilon^{zx}_{lmn} \sin \pi l h_1 \cos \pi m h_2 \sin \pi n h_3\big|. \end{aligned} \quad (4)$$

The integers l, m, n define a particular site and h_1, h_2, h_3 are the usual Miller indices. The Fourier coefficients α, γ, δ, ε, obtained by Fourier transforms, give information in real space on the atomic configuration (α) and on the displacement field ($\gamma, \delta, \varepsilon$). The α_{lmn} are the Warren–Cowley parameters (Cowley, 1950) defined by

$$\alpha_{lmn} = 1 - \frac{P^{AB}_{lmn}}{C_B},$$

where P^{AB}_{lmn} is the conditional probability of finding a B atom at site lmn when the origin is occupied by an A atom. The other Fourier coefficients are given by

$$\begin{aligned} \gamma^x_{lmn} &= 2\pi \big| F_{AA} \langle x^{AA}_{lmn} \rangle + F_{AB} \langle x^{AB}_{lmn} \rangle + F_{BB} \langle x^{BB}_{lmn} \rangle \big| \\ \delta^x_{lmn} &= -2\pi^2 \big| F_{AA} \langle (x^{AA}_{lmn})^2 \rangle + F_{AB} \langle (x^{AB}_{lmn})^2 \rangle \\ &\quad + F_{BB} \langle (x^{BB}_{lmn})^2 \rangle \big| \\ \varepsilon^{xy}_{lmn} &= -4\pi^2 \big| F_{AA} \langle (x^{AA}_{lmn} y^{AA}_{lmn}) \rangle + F_{AB} \langle (x^{AB}_{lmn} y^{AB}_{lmn}) \rangle \\ &\quad + F_{BB} \langle (x^{BB}_{lmn} y^{BB}_{lmn}) \rangle \big|, \end{aligned}$$

where

$$F_{AA} = \frac{f_A^2}{(f_A - f_B)^2} \left(\frac{C_A}{C_B} + \alpha_{lmn} \right)$$

$$F_{AB} = \frac{2 f_A f_B}{(f_A - f_B)^2} (1 - \alpha_{lmn})$$

$$F_{BB} = \frac{f_B^2}{(f_A - f_B)^2} \left(\frac{C_B}{C_A} + \alpha_{lmn} \right).$$

The coefficients γ^y_{lmn}, γ^z_{lmn}, δ^y_{lmn}, δ^z_{lmn}, ε^{yz}_{lmn} and ε^{zx}_{lmn} are expressed similarly. The quantity $\langle x^{uv}_{lmn} \rangle$ denotes the average displacement along the [100] axis between u–v atom pairs separated by the vector $\mathbf{r}_{lmn}$ ($\mathbf{r}_{lmn} = l\mathbf{a}_1/2 + m\mathbf{a}_2/2 + n\mathbf{a}_3/2$, where $\mathbf{a}_1$, $\mathbf{a}_2$, $\mathbf{a}_3$ are the translation vectors of the cubic unit cell).

In the Borie & Sparks (1971) treatment, the different terms of the intensity [(1)] are separated without any correction; the dynamic displacements are only assumed to be a non-separable contribution to the second-order intensity I_2.

By performing an expansion of the intensity up to the third order, a correction by a temperature factor – similar to a Debye–Waller one – which decreases the value of the scattering factor f_A to $f_A \exp(-W_A)$ (Bardhan & Cohen, 1976) may be introduced (Hayakawa, Bardhan & Cohen, 1975).

Another way of correcting dynamic displacement prior to any separation of the total intensity consists in either accounting for the elastic effect of thermal motion of a Debye–Waller factor and the inelastic effect (TDS: thermal diffuse scattering) by the procedure of Walker & Chipman (1970), or making measurements at two different temperatures and assuming that the TDS varies linearly with temperature (Borie & Sparks, 1964). The intensity is then extrapolated at each point of reciprocal space to absolute zero.

In the present context, these different ways of correction of the raw intensity are compared with respect to the resulting α parameters (Table 1 and Fig. 2).

There is a continuous variation of α′ values from the method without any correction – neither Debye–Waller nor TDS – to the extrapolated one. The correction using the calculation of Walker & Chipman (1970) is too low; it is specially noteworthy in the measurements made at room temperature. This TDS correction is based on the elastic constants C_{11}, C_{12} and C_{44} extrapolated from the known values of Cu, Au (Kittel, 1972) and Cu_3Au (Flinn, Mac Manus & Rayne, 1960). The Debye–Waller factor is calculated from the Debye temperature (θ_D = 186 K) measured by Martin (1976). In the present case, the calculated correction is too small; this may be explained by the fact that the contributions from optic modes and multi-phonon processes – which are weak but which vary very slowly – are neglected. Another source of error comes from the fact that the calculation is applied to regions of reciprocal space far away from Bragg peaks (corresponding to long-wavelength phonons).

Finally, the best method to correct intensity from thermal effects seems to be the extrapolation at 0 K: with this method, the value of $\alpha_0 = 1{\cdot}041$ is the closest to 1 (theoretical value).

In conclusion the results given in the next section are analyzed following the flow chart of Fig. 3. The scattering factors f are taken from Doyle & Turner (1968) and the corrections f' and f'' from Dauben & Templeton (1955). The points which are not measured around the Bragg peaks are extrapolated after separation of the SRO intensity. We have tried different ways of extrapolating the SRO intensity as was reported by Moss (1966*a*) (in the discussion of the Sparks & Borie paper). We have chosen to keep the minimum value

Table 1. *Warren–Cowley parameters α_{lmn} obtained from the different analysis methods*

		Experiment made at 77 K		Experiment made at room temperature		
	Linearized extrapolation to 0 K	with TDS correction	without TDS correction	with TDS correction	without TDS correction	Sparks & Borie 'true' method without Debye–Waller correction
l m n	The scattering factor is corrected from Debye–Waller term					
0 0 0	1·041	1·117	1·152	1·2018	1·3311	1·4204
1 1 0	−0·933	−0·101	−0·099	−0·1118	−0·1052	−0·0084
2 0 0	0·2	−0·1942	0·187	0·1886	0·1596	0·1639
2 1 1	−0·0486	−0·0503	−0·053	−0·0495	−0·058	−0·0641
2 2 0	0·094	0·1027	0·102	0·1187	0·1135	0·1017
3 1 0	−0·0279	−0·0296	−0·031	−0·0364	−0·0434	−0·0467
2 2 2	0·0693	0·071	0·073	0·073	0·0819	0·0770
3 2 1	−0·019	−0·0177	−0·016	−0·0178	−0·013	−0·0168
4 0 0	0·0588	0·0513	0·053	0·0479	0·0545	0·0529
4 1 1	−0·0213	−0·022	0·021	0·0185	−0·0142	−0·0151
3 3 0	−0·0021	0·0004	0·002	0·0007	0·0083	0·0073
4 2 0	0·0439	0·0456	0·046	0·0489	0·0508	0·0504
3 3 2	−0·0108	−0·0109	−0·011	−0·0126	−0·0110	−0·0107
4 2 2	0·0345	0·0348	0·035	0·0376	0·0353	0·0352
5 1 0	−0·0066	−0·0037	−0·003	−0·0043	−0·0007	0·0009
4 3 1	−0·0100	−0·0126	−0·013	−0·0138	−0·0139	−0·0118
5 2 1	−0·0073	−0·0072	−0·007	−0·0078	−0·008	−0·0062
4 4 0	0·026	0·0236	0·023	0·0256	0·0217	0·0229
5 3 0	−0·0074	−0·0062	−0·007	−0·0057	−0·0081	−0·0063
4 3 3	−0·0088	−0·0101	−0·011	−0·0123	−0·0135	−0·0015

near the Bragg peak up to its exact position. As was explained by Moss & Clapp (1968) the SRO intensity does not tend to a specific value at the position of the Bragg peak.

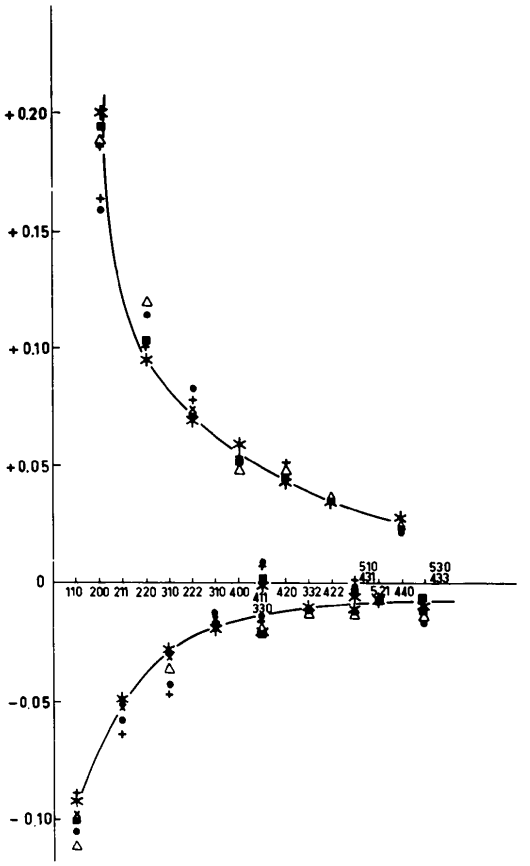

Fig. 2. Comparison of Warren–Cowley parameters. Room-temperature experiment: + Sparks & Borie 'true' method without any correction (neither TDS nor Debye–Waller factor); ● without TDS correction, with correction of Debye–Waller factor; △ with TDS correction, with correction of Debye Waller factor. Experiment made at 77 K: × without TDS correction; ■ with TDS correction. * Extrapolation to 0 K.

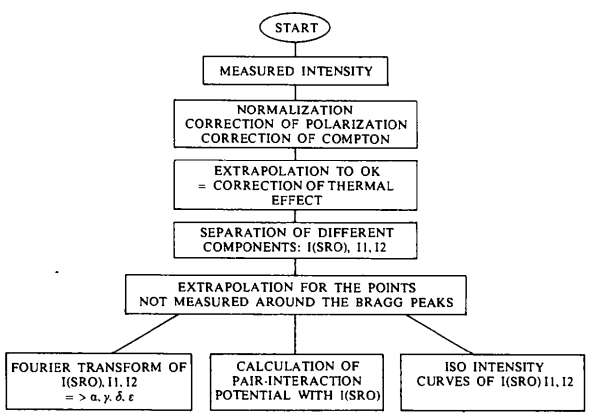

Fig. 3. Flow chart of analysis.

Results and interpretation

(a) *General*

Fig. 4 shows the diffuse X-ray intensity distribution observed on the $(h_1,h_2,0)$ reciprocal-lattice plane; the intensities are expressed in Laue monotonic units. As was found by Batterman (1957), this intensity shows the presence of the size-effect modulation: the maxima of intensities, displaced from the positions 100 and 110, are increasingly asymmetric, with the h value: hence the correction of size-effect modulation on the intensity is large and must be made carefully.

(b) *The nature of SRO*

The distribution of SRO intensity (I_{SRO}) is obtained after performing the separation of the terms of the total diffuse intensity as described in the flowchart (Fig. 3). The result on the $(h_1,h_2,0)$ reciprocal plane is shown in Fig. 5. At the 110 and 100 positions a fourfold splitting of diffuse scattering can be seen. The splitting separation is nearly $m = 1/20$ r.l.u. as confirmed by electron diffraction performed on the same crystal (Fig. 6). This result agrees with the earlier observation on evaporated thin films (Watanabe & Fischer, 1965).

From diffusion patterns of SRO intensity in the planes (h_1,h_2,w) the intensity distribution in reciprocal space can be inferred as shown in Fig. 7. We note the elongation of the split spots along the ⟨100⟩ directions.

By performing the Fourier inversion of the intensity, α_{lmn} parameters are calculated up to the 112th shell (Table 2). The values of α_{lmn} are plotted *versus* r_{lmn} (Fig. 2). The sign and the variation of α_{lmn} are similar to

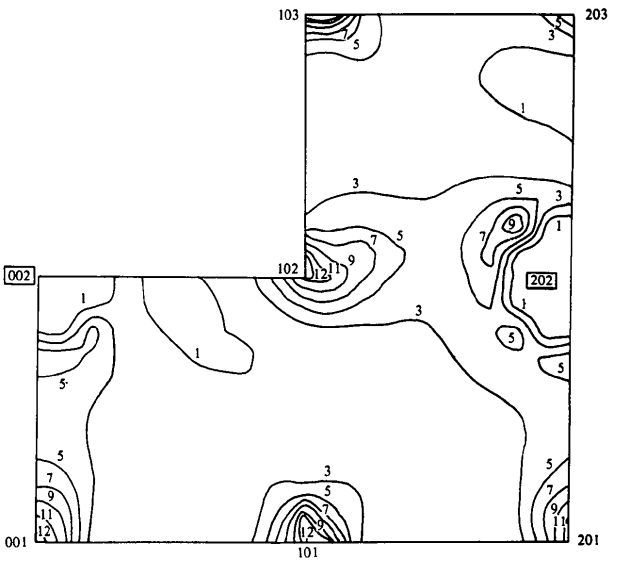

Fig. 4. Experimental isointensity map of total scattering in Laue monotonic units for $h_2 = 0$ reciprocal-lattice plane (Au_3Cu).

Table 2. *Experimental values of SRO parameters*

C	l m n	α	C	l m n	α	C	l m n	α	C	l m n	α	C	l m n	α
0	0 0 0	1·04042	28	7 3 0	−0·00380	48	10 1 1	−0·00259	65	10 6 2	0·00022	86	11 8 3	0·00253
1	1 1 0	−0·09319	29	6 5 1	−0·00132	49	8 6 2	0·00075	66	9 6 5	−0·00023	87	9 9 6	0·00019
2	2 0 0	0·19983	29	7 3 2	−0·00240	49	10 2 0	0·00116	67	8 8 4	−0·00306	87	10 7 7	−0·00170
3	2 1 1	−0·04852	30	8 0 0	0·01254	50	9 5 0	−0·00357	68	9 7 4	−0·00303	88	10 10 0	−0·00531
4	2 2 0	0·09384	31	7 4 1	−0·00051	50	9 4 3	−0·00110	68	9 8 1	0·00589	88	10 8 6	−0·00145
5	3 1 0	−0·02782	31	5 5 4	−0·00342	51	6 6 6	−0·00103	68	11 4 3	−0·00110	89	11 9 0	−0·00688
6	2 2 2	0·06920	31	8 1 1	−0·00174	51	10 2 2	0·00071	68	11 5 0	−0·00357	90	10 10 2	−0·00732
7	3 2 1	−0·01893	32	6 4 4	0·00623	52	7 6 5	0·00049	69	10 7 1	0·00451	91	11 7 6	−0·00181
8	4 0 0	0·05871	32	8 2 0	0·00828	52	9 5 2	−0·00330	69	10 5 5	0·00337	91	10 9 5	0·00130
9	3 3 0	−0·00211	33	6 5 3	−0·00021	52	10 3 1	−0·00032	69	11 5 2	−0·00330	91	11 9 2	−0·00788
9	4 1 1	−0·02136	34	6 6 0	0·00967	53	8 5 5	0·00022	70	10 6 4	0·00139	92	11 8 5	0·00176
10	4 2 0	0·04380	34	8 2 2	0·00504	53	8 7 1	0·00444	71	9 8 3	0·00253	93	10 10 4	0·00071
11	3 3 2	−0·01079	35	7 4 3	−0·00011	53	7 7 4	−0·00428	72	10 7 3	0·00599	94	11 9 4	−0·00486
12	4 2 2	0·03451	35	7 5 0	−0·00364	54	8 6 4	−0·00013	72	11 6 1	0·00459	95	11 10 1	0·00702
13	4 3 1	−0·01008	35	8 3 1	−0·00038	54	10 4 0	0·00155	73	8 7 7	0·00190	96	9 9 8	−0·00062
13	5 1 0	−0·00661	36	6 6 2	0·00447	55	10 3 3	−0·00293	73	11 5 4	−0·00207	97	10 8 8	−0·00349
14	5 2 1	−0·00731	37	7 5 2	−0·00321	55	9 6 1	0·00459	73	9 9 0	−0·00688	98	10 9 7	0·00320
15	4 4 0	0·02606	38	8 4 0	−0·00045	56	10 4 2	0·00050	74	8 8 6	−0·00041	98	11 10 3	0·00474
16	4 3 3	−0·00878	39	8 3 3	0·00087	57	9 5 4	−0·00207	74	10 8 0	−0·00605	99	11 8 7	−0·00094
16	5 3 0	−0·00735	39	9 1 0	−0·00471	57	8 7 3	0·00098	75	9 7 6	−0·00181	100	10 10 6	0·00263
17	4 4 2	0·01767	40	8 4 2	0·00256	57	11 1 0	−0·00471	75	9 9 2	−0·00788	101	11 9 6	0·00019
17	6 0 0	0·01512	41	7 6 1	0·00120	58	10 5 1	0·00138	75	11 6 3	0·00266	102	11 11 0	−0·00688
18	5 3 2	−0·00700	41	6 5 5	0·00031	58	9 6 3	0·00266	76	10 8 2	−0·00190	103	11 10 5	0·00130
18	6 1 1	−0·00982	41	9 2 1	0·00110	58	11 2 1	0·00110	77	9 8 5	0·00176	103	11 11 2	−0·00788
19	6 2 0	0·01330	42	6 6 4	0·00082	59	8 8 0	−0·00490	77	11 7 0	−0·00806	104	11 11 4	−0·00486
20	5 4 1	−0·00618	43	7 5 4	−0·00248	60	9 7 0	−0·00806	78	10 6 6	0·00112	105	10 9 9	0·00060
21	6 2 2	0·01269	43	8 5 1	0·00201	60	11 3 0	−0·00033	79	10 7 5	0·00230	106	10 10 8	0·00189
22	6 3 1	−0·00699	43	9 3 0	−0·00033	61	8 8 2	−0·00223	79	11 7 2	−0·00390	107	11 9 8	−0·00062
23	4 4 4	0·01458	44	7 6 3	−0·00070	61	10 4 4	−0·00396	80	9 9 4	−0·00486	108	11 10 7	0·00320
24	5 5 0	−0·00486	44	9 3 2	−0·00169	62	7 7 6	0·00168	81	10 8 4	−0·00190	109	11 11 6	0·00019
24	5 4 3	−0·00356	45	8 4 4	0·00163	62	9 7 2	−0·00390	82	10 9 1	0·00702	110	10 10 10	−0·00195
24	7 1 0	−0·00236	46	7 7 0	−0·000619	62	10 5 3	0·00235	82	11 6 5	−0·00023	111	11 10 9	0·00060
25	6 4 0	0·00763	46	8 5 3	0·00179	62	11 3 2	−0·00169	83	11 7 4	−0·00303	112	11 11 8	−0·00062
26	5 5 2	−0·00230	46	9 4 1	0·00060	63	8 6 6	0·00271	83	11 8 1	0·00589			
26	6 3 3	−0·00186	47	8 6 0	−0·00344	63	10 6 0	−0·00809	84	10 9 3	0·00474			
26	7 2 1	−0·00125	47	10 0 0	−0·00074	64	8 7 5	0·00039	85	8 8 8	−0·00118			
27	6 4 2	0·00907	48	7 7 2	−0·00449	64	11 4 1	0·00060	86	9 8 7	−0·00094			

those obtained for Ni_3Fe (Lefebvre, Bley, Bessière, Fayard, Roth & Cohen, 1980) and Cu_3Pd (Ohshima, Watanabe & Harada, 1976) but the absolute magnitude decreases more slowly with the interatomic distance.

To investigate how the fine structure of SRO diffuse scattering is reflected in the values of α_{lmn}, the diffuse intensity map is synthesized using the previous values of α_{lmn}. Figs. 8(*a*), (*b*) and (*c*) show examples of the recalculated intensity map with, respectively 45, 69 and 112 terms: a qualitatively good fitting requires

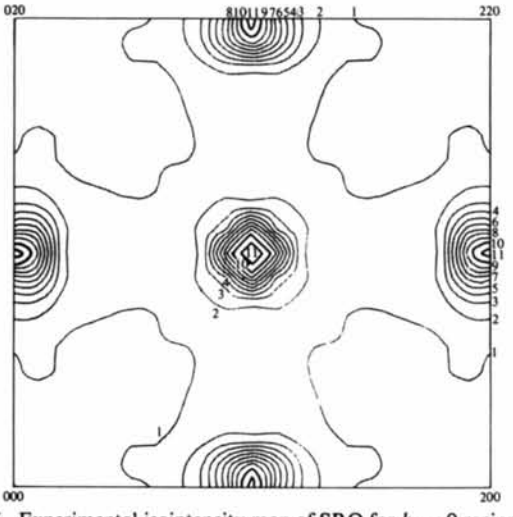

Fig. 5. Experimental isointensity map of SRO for $h_2 = 0$ reciprocal-lattice plane (Au_3Cu).

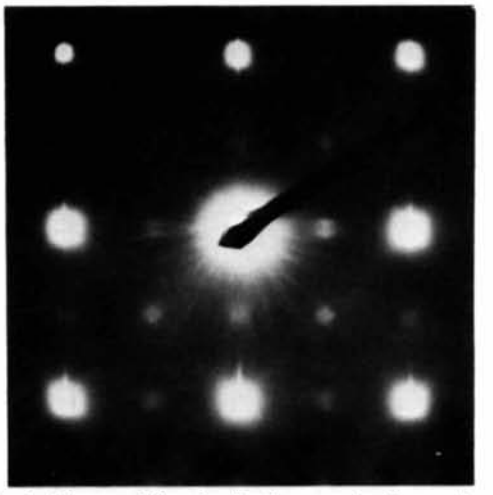

Fig. 6. Electron diffraction for the same Au_3Cu sample.

at least 69 terms. The characteristic splitting of the fine structure of diffuse intensity is induced by the high-order α_{lmn} parameters, although their absolute values are small compared with those of the lower-order parameters.

The fact that many terms are needed is directly correlated with the splitting distance m: in Cu_3Pd where the m value is larger ($m = 0{\cdot}13$) only 47 terms are needed to synthesize the fine structure of the diffuse intensity. The smaller the value of m is, the greater is the number of α_{lmn} terms required for a proper fitting of the diffuse intensity.

(c) *Determination of the pair-interaction potential*

The only way interatomic potentials may easily be calculated from the SRO diffuse intensity follows from the so-called mean field approximation (Clapp & Moss, 1966) where the intensity and the Fourier coefficients of the interatomic potentials are related by

$$I(k) = \frac{C}{1 + 2\,C_A C_B \beta V(k)}, \qquad (5)$$

where $V(k)$ is the Fourier transform of the pair-interaction potential, $V_{lmn} = \frac{1}{2}(V^{AA}_{lmn} + V^{BB}_{lmn} - 2V^{AB}_{lmn})$, between pairs of atoms separated by a vector $\mathbf{r}_{lmn}$ and $\beta = 1/k_B T$ with k_B the Boltzman constant and T the temperature. C is a normalization constant which can be determined by the additional condition $V_{000} = 0$, leading to

$$C = V_m / \int_{\text{cell}} \mathrm{d}^3k / I(k) \qquad (6)$$

where V_m is the cell volume.

Through (5) and (6) the values of $V(k)$ can be obtained directly from the measured SRO diffuse intensity after smoothing around the Bragg peak as described in *Data analysis*. As already noted by Ohshima *et al.* (1976), a small error in the observed diffuse intensity away from the diffuse peak [*i.e.* near the fundamental reflexion where $I(k)$ is small] may result in a large error in $V(k)$.

The isointensity curves of $V(k)$ in a plane $(h_1,h_2,0)$ (Fig. 9) show the same particular feature as the isointensity curves of the SRO diffuse intensity. A fourfold splitting is seen at the 110 and 100 positions.

The pair-interaction potentials V_{lmn} can be determined by Fourier inversion of $V(k)$. $V(k)$ has been obtained either from the experimental I_{SRO}, or from the I_{SRO} synthesized with the α_{lmn} parameters up to the 112th shell (Table 3). The ratios V_{lmn}/V_{110} for the

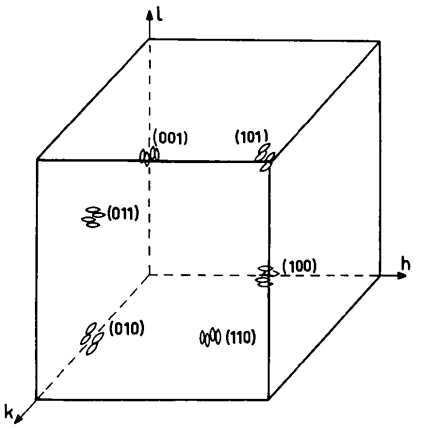

Fig. 7. Intensity distribution in reciprocal space.

Table 3. *Values of pair-interaction potentials*

		With I(SRO) measured		With I(SRO) synthesized with α parameters up to the 112th shell	
C	$l\,m\,n$	V_{lmn} (meV)	V_{lmn}/V_{110}	V_{lmn} (meV)	V_{lmn}/V_{110}
0	0 0 0	0·112	0·016	0·104	0·014
1	1 1 0	6·812	1·	7·540	1·
2	2 0 0	−11·184	−1·642	−10·320	−1·369
3	2 1 1	1·680	0·247	1·095	0·145
4	2 2 0	0·787	0·116	0·379	0·050
5	3 1 0	0·261	0·038	0·302	0·040
6	2 2 2	−0·962	−0·141	−2·801	−0·371
7	3 2 1	−0·198	−0·029	−0·523	−0·069
8	4 0 0	−0·027	−0·004	1·486	0.197
9	3 3 0	−1·481	−0·217	−0·430	−0·057
9	4 1 1	0·022	0·003	0·453	0·060
10	4 2 0	−0·324	−0·048	0·459	0·061

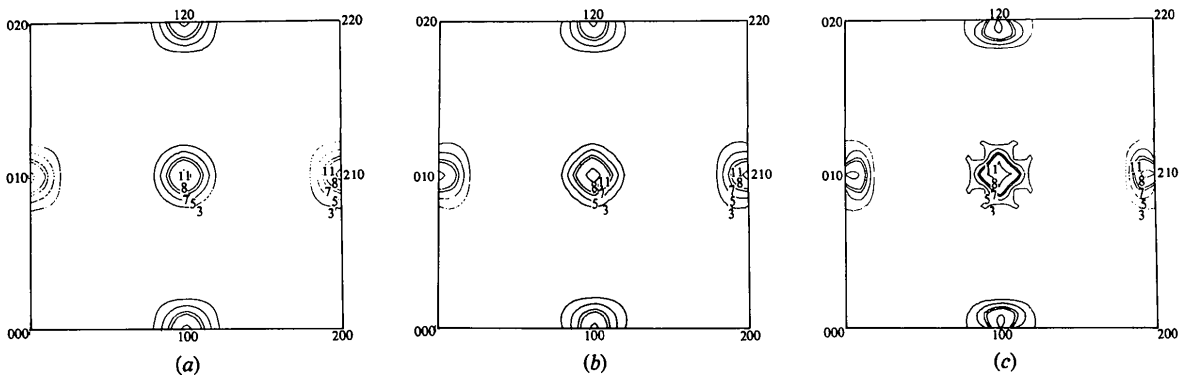

Fig. 8. Diffuse scattering isointensity map synthesized from experimental α_{lmn} parameters; (*a*) up to the 45th shell, (*b*) up to the 69th shell, (*c*) up to the 112th shell.

second method are plotted *versus* the interatomic distance r_{lmn} (Fig. 10). These results are similar to those obtained on Cu_3Pd: the pair-interaction potential is of relatively long range and oscillates with the distance. As with the α_{lmn} parameters, the diffuse intensity map was recalculated using the values given in Table 3 (second method). With the four potentials V_{110}, V_{200}, V_{211} and V_{220}, the SRO diffuse intensity is roughly restored (Fig. 11). The 'egg-shape' fine structure of the SRO diffuse intensity can be obtained by including more potentials: with ten potentials the elongation along the [100] axis appears.

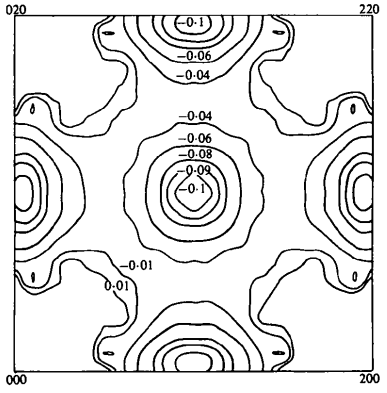

Fig. 9. Potential isointensity map for $h_2 = 0$ reciprocal-lattice plane.

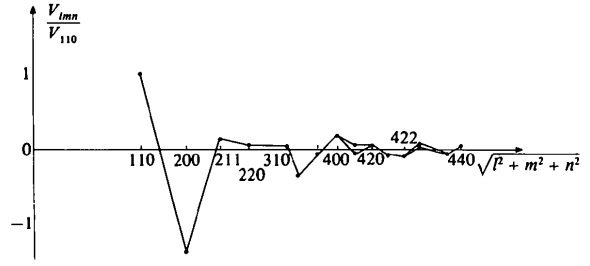

Fig. 10. Pair interaction potential ratio V_{lmn}/V_{110} *vs* interatomic distance.

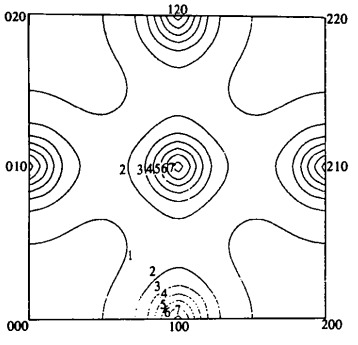

Fig. 11. Diffuse scattering isointensity map synthesized from pair interaction potential up to V_{220}.

The first two ratios $V_{200}/V_{110} = -1{\cdot}37$ and $V_{211}/V_{110} = 0{\cdot}14$ are quite different from the values used by Moss & Clapp (1968) ($V_{200}/V_{110} = -1{\cdot}2$, $V_{211}/V_{110} = 0{\cdot}9$) by fitting only the first ten α_{lmn} parameters experimentally obtained by Batterman (1957) with the α_{lmn} parameters given by the Fourier transform of the SRO intensity derived from these two ratios V_{200}/V_{110} and V_{211}/V_{110} only. The large value of V_{211} they obtained may be due to the initial truncation they made in neglecting all V_{lmn} ($lmn > 211$). Actually, as in the case of Cu_3Pd (Ohshima *et al.*, 1976) more potentials are required to reproduce the SRO intensity profile. In particular the elongation along [100] of the diffuse intensity is probably due to high-order pair-interaction parameters (and not solely to the high value of V_{211}).

(*d*) *Effect of atomic displacement*

Fig. 12 shows the intensity distribution of the diffuse scattering due to the size effect I_1 [see (1)]. The atomic displacement parameters γ^x_{lmn}, γ^y_{lmn}, γ^z_{lmn} are obtained by performing the Fourier transformation of I_1 (Table 4). The γ values are of the same order as those of Cu_3Pd (Ohshima *et al.*, 1976) and Cu_3Au (Bardhan & Cohen, 1976). They are of opposite sign in relation to the atomic concentration of the larger atom. For both Cu–Pd and Cu–Au alloys the cell parameter increases with increasing concentration of Pd or Au respectively.

The intensity of the diffuse scattering due to the effect of second order for atomic displacement (I_2) is very weak and only the first ten values of δ parameters (Table 4) are given; they are always lower than the γ ones. The values are so weak that they fall within the range of error.

Here the effect of atomic displacement is considered only as a correction of I_{SRO}. Without this correction the exact form of fourfold splitting of the diffuse scattering is not seen.

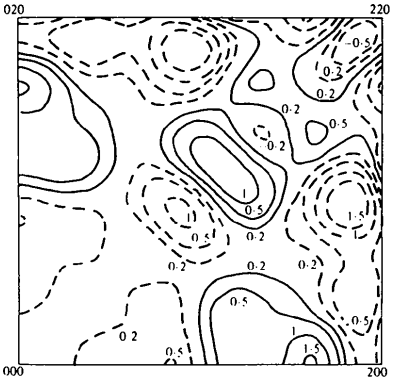

Fig. 12. Diffuse scattering isointensity map due to size effect I_1.

Table 4. *Experimental values of displacement parameters*

C l m n	γ_x	γ_y	γ_z	δ_x	δ_y	δ_z
0 0 0 0	–	–	–	0·0974	0·0974	0·0974
1 1 1 0	−0·0956	−0·0956	–	0·0078	0·0078	0·0238
2 2 0 0	0·0709	–	–	−0·0204	0·0218	−0·0204
3 2 1 1	0·0114	−0·0240	−0·0240	−0·0107	0·0052	0·0052
4 2 2 0	0·0196	0·0196	–	−0·0034	−0·0034	0·0116
5 3 1 0	0·0008	−0·0098	–	−0·0057	0·0013	0·0059
6 2 2 2	0·0185	0·0185	0·0185	0·0009	0·0009	0·0009
7 3 2 1	−0·0003	0·0062	−0·0030	−0·0023	−0·0003	0·0018
8 4 0 0	0·0409	–	–	−0·0062	0·0009	0·0009
9 4 1 1	0·0092	−0·0032	−0·0032	−0·0042	−0·0004	−0·0004
9 3 3 0	0·0010	0·0010	–	−0·0013	−0·0013	0·0026
10 4 2 0	0·0288	0·0139	–	−0·0039	–	0·0007

Discussion

X-ray diffuse scattering experiments on an Au_3Cu single crystal rapidly cooled from 483 K show a characteristic fourfold splitting around the positions of the superlattice reflexions. Such a splitting has been often reported by electron diffraction on disordered alloys: Au_3Cu (Watanabe & Fischer, 1965); Cu_3Au (Raether, 1952; Marcinkowski & Zwell, 1963; Hashimoto & Ogawa, 1970); CuAu (Sato *et al.*, 1962); CuPt and CuPd (Ohshima & Watanabe, 1973).

Previous X-ray diffuse scattering of Au_3Cu (Batterman, 1957) showed only egg-shaped diffuse intensity peaks with no splitting since the resolution of the spectrometer and the separation of the contribution for atomic displacements to the intensity were not good enough. In other disordered alloys, the splitting was observed by X-ray diffuse scattering; essentially in: Cu_3Au (Moss, 1966*a*,*b*; Bardhan & Cohen, 1976); Au–40 at.% Pd (Linn *et al.*, 1970); Cu–14·76 at.% Al (Epperson *et al.*, 1978); Cu_3Pd (Ohshima *et al.*, 1976).

The Cu_3Pd study is the only case where the fourfold splitting has been synthesized from the measured α_{lmn} parameters up to the 47th-neighbour shell. For CuAl a synthesized map with fourfold splitting has been also obtained using, in this case, the modelled α_{lmn} parameters – computed with the Gehlen & Cohen (1965) method up to the 69th-neighbour shell.

In the present study, too, fairly high-order α_{lmn} parameters – such as those beyond the 69th-neighbour shell – are needed to reproduce the fine structure. This merely means that much harmonic information is required to recreate structure at non-rational positions in reciprocal space.

The splitting shown in disordered Cu_3Au (Bardhan & Cohen, 1976) is like the Au_3Cu one but there is no elongation of the split spot along the [100] direction. Moss & Clapp (1968) attribute this elongation to the increasing importance of V_{211}/V_{110} with a correspondingly diminished V_{200}/V_{110}. But, as we have already discussed, this qualitative agreement may be only due to the small number of neighbours used in the model. Moreover, the mean field theory used by Moss & Clapp (1968) cannot reproduce the diffuse satellites.

For Au_3Cu the similarity in the aspects between the fourfold splitting above T_c and the diffraction due to the PAP structure below T_c brings forward the question as to whether or not there is a relation between the SRO state above T_c and the PAP structure below T_c. As the (Cu,Au) phase diagram does not present a PAP structure for stoichiometric Cu_3Au it seems that a direct relation does not exist.

An interpretation has been provided by the Fermi-surface-imaging theory of Moss (1969) and Moss & Walker (1974). Consideration of the pair-interaction potential in a disordered alloy through conduction electrons leads to an explanation of how the Fermi surface of a disordered alloy is reflected in a local-order diffuse scattering of X-rays, electrons and neutrons, through anomalies similar to those predicted by Kohn for phonon scattering. If the interatomic potential $V(\mathbf{k})$ is caused by conduction electrons in an alloy, it has singularities at $\mathbf{k} = 2\mathbf{k}_F + \mathbf{G}$, where $\mathbf{k}$ is a wave vector, $\mathbf{k}_F$ corresponds to the Fermi surface and $\mathbf{G}$ is a reciprocal-lattice vector. Following this theory, a splitting separation of near 1/20 r.l.u. is expected for Au_3Cu (Moss, 1969) in agreement with the one that has been observed in the present study.

However, for a quantitative interpretation exact values of pair-interaction potentials are needed. The calculation of the pair-interaction potentials by (5) is made with an approximate method (Bragg–Williams approximation) which may not be valid within 10% of the ordering temperature. So experiments are in progress on samples quenched from higher temperatures where more reliable values of pair-interaction potentials are expected.

On the other hand, the restriction of the theory in using pair-wise interactions and two-site correlation parameters probably constitutes a serious limitation. In fact, the phase diagram for Cu–Au alloys is not symmetrical about the equiatomic concentration, suggesting three – or more – atom interactions, or a variation of $V(r)$ with concentration.

Recently, a different approach was developed by Sanchez (1982) using the cluster variation method (CVM). It is expected that the CVM will result in more accurate potentials. Furthermore, many body interactions can be included within the framework of the CVM and consequently these interactions would be evaluated.

The authors wish to thank P. Favreau for preparing the Au_3Cu single crystal, J. P. Chevalier for the electron diffraction diagram and D. Gratias for helpful discussions. They are particularly grateful to F. Bley for her help in setting the crystal and adapting computer programs.

References

BARDHAN, P. & COHEN, J. B. (1976). *Acta Cryst.* A**32**, 597–613.
BATTERMAN, B. W. (1957). *J. Appl. Phys.* **28**, 556–561.
BESSIÈRE, M., LEFEBVRE, S., CALVAYRAC, Y., BLEY, F. & FAYARD, M. (1982). *J. Appl. Cryst.* **15**, 94–97.
BORIE, B. & SPARKS, C. J. (1964). *Acta Cryst.* **17**, 827–835.
BORIE, B. & SPARKS, C. J. (1971). *Acta Cryst.* A**27**, 198–201.
CLAPP, P. C. & MOSS, S. C. (1966). *Phys. Rev.* **142**, 418–427.
COWLEY, J. M. (1950). *J. Appl. Phys.* **21**, 24–30.
CROMER, D. T. & MANN, J. B. (1967). *J. Chem. Phys.* **47**, 1892–1893.
DAUBEN, H. & TEMPLETON, D. H. (1955). *Acta Cryst.* **8**, 841–842.
DOYLE, P. A. & TURNER, P. S. (1968). *Acta Cryst.* A**24**, 390–397.
EPPERSON, J. E., FÜRNROHR, P. & ORTIZ, C. (1978). *Acta Cryst.* A**34**, 667–681.
FLINN, P. A., MAC MANUS, G. M. & RAYNE, J. A. (1960). *J. Phys. Chem. Solids*, **15**, 189–195.
GEHLEN, P. & COHEN, J. B. (1965). *Phys. Rev.* **139**, A844–A855.
GRAGG, J. E. & COHEN, J. B. (1971). *Acta Metall.* **19**, 507–519.
GRATIAS, D., CONDAT, M. & FAYARD, M. (1972). *Phys. Status. Solidi. A*, **14**, 123–128.
HASHIMOTO, S. & OGAWA, S. (1970). *J. Phys. Soc. Jpn*, **29**, 710–721.
HAYAKAWA, M., BARDHAN, P. & COHEN, J. B. (1975). *J. Appl. Cryst.* **8**, 87–95.
HIRABAYASHI, M. (1959). *J. Phys. Soc. Jpn*, **14**, 262–273.
KITTEL, C. (1972). *Introduction à la Physique du Solide*, p. 147. Paris: Dunod.
LEFEBVRE, S., BLEY, F., BESSIÈRE, M., FAYARD, M., ROTH, M. & COHEN, J. B. (1980). *Acta Cryst.* A**36**, 1–7.
LINN, W., SPRUIELL, J. E. & WILLIAMS, R. O. (1970). *J. Appl. Cryst.* **3**, 297–305.
MARCINKOWSKI, M. J. & ZWELL, L. (1963). *Acta Metall.* **11**, 373–390.
MARTIN, D. L. (1976). *Phys. Rev. B*, **14**, 369–385.
MOSS, S. C. (1966*a*). Discussion on C. J. Sparks & B. Borie's paper in *Local Atomic Arrangements Studied by X-ray Diffraction*, edited by J. B. COHEN & J. E. HILLIARD, p. 47. New York: Gordon & Breach.
MOSS, S. C. (1966*b*). *Local Atomic Arrangements Studied by X-ray Diffraction*, edited by J. B. COHEN & J. E. HILLIARD, pp. 95–122. New York: Gordon & Breach.
MOSS, S. C. (1969). *Phys. Rev. Lett.* **22**, 1108–1111.
MOSS, S. C. & CLAPP, P. C. (1968). *Phys. Rev.* **171**, 764–777.
MOSS, S. C. & WALKER, R. H. (1974). *J. Appl. Cryst.* **8**, 96–107.
OHSHIMA, K. & WATANABE, D. (1973). *Acta Cryst.* A**29**, 520–526.
OHSHIMA, K., WATANABE, D. & HARADA, J. (1976). *Acta Cryst.* A**32**, 883–892.
PEARSON, W. B. (1958). *A Handbook of Lattice Spacings and Structures of Metals and Alloys*. Oxford: Pergamon.
RAETHER, H. (1952). *Angew. Phys.* **4**, 53–59.
SANCHEZ, J. M. (1982). *Physica (Utrecht) A*. In the press.
SATO, K. & TOTH, R. S. (1966). *J. Appl. Phys.* **37**, 3367–3370.
SATO, K., WATANABE, D. & OGAWA, S. (1962). *J. Phys. Soc. Jpn*, **17**, 1647–1651.
WALKER, C. B. & CHIPMAN, D. R. (1970). *Acta Cryst.* A**26**, 447–455.
WATANABE, D. & FISCHER, P. M. J. (1965). *J. Phys. Soc. Jpn*, **20**, 2170–2179.

Acta Cryst. (1983). B**39**, 153–157

Structure of 'Orange' $^{18}O_2$ at 9·6 GPa and 297 K*

BY DAVID SCHIFERL, DON T. CROMER, LARRY A. SCHWALBE AND ROBERT L. MILLS

University of California, Los Alamos National Laboratory, Los Alamos, New Mexico 87545, *USA*

(*Received* 3 *May* 1982; *accepted* 21 *September* 1982)

Abstract

A single crystal of 'orange' $^{18}O_2$ at 9·6 (3) GPa and 297 (1) K was produced in a Merrill–Bassett diamond-anvil high-pressure cell and examined by X-ray diffraction. Pressure was determined with the ruby-fluorescence method. The unit cell is orthorhombic, space group *Fmmm*, lattice constants $a = 4{\cdot}2151$ (6), $b = 2{\cdot}9567$ (4), $c = 6{\cdot}6897$ (17) Å, molar volume = $12{\cdot}56 \times 10^{-6}$ m^3 mol^{-1} with four molecules per unit cell. The charge densities of the molecules overlap or distort to a considerable degree. Generalized scattering factors were used in an aspherical-atom least-squares refinement. For five refined parameters and 24 observations the final R_w is 0·056. A correction is made to our previous work on β-O_2 at 5·5 GPa and 299 K.

Introduction

Diamond-cell technology has made possible the detailed study of solidified gases at ultrahigh pressure. Recently Nicol, Hirsch & Holzapfel (1979) carried out optical observations on solid O_2 in a diamond cell over the range $248 < T < 323$ K and $5{\cdot}0 < P < 18{\cdot}0$ GPa (1 GPa = 10 kbar) that show a surprisingly complex behavior. At 298 K they found that oxygen freezes at 5·9 GPa and then at 9·6 and 9·9 GPa undergoes transitions marked by dramatic color changes.

* Work performed under the auspices of the US Department of Energy.

0567-7408/83/020153-05$01.50